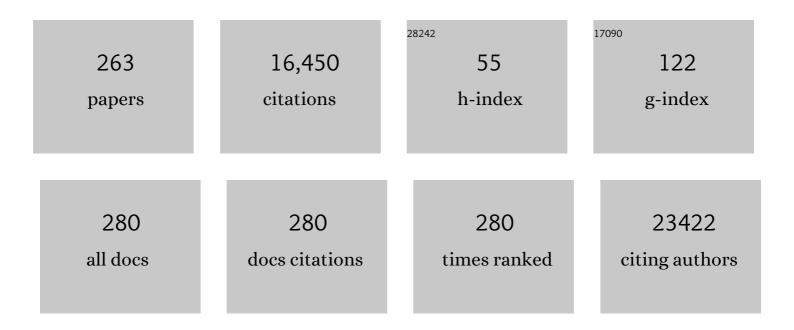
List of Publications by Year in descending order

Source: https://exaly.com/author-pdf/243717/publications.pdf Version: 2024-02-01



**САДАН НАІСН** 

#	Article	IF	CITATIONS
1	Vertical field-effect transistor based on graphene–WS2 heterostructures for flexible and transparent electronics. Nature Nanotechnology, 2013, 8, 100-103.	15.6	1,543
2	Light-emitting diodes by band-structure engineering in van der Waals heterostructures. Nature Materials, 2015, 14, 301-306.	13.3	1,397
3	Tunable sieving of ions using graphene oxide membranes. Nature Nanotechnology, 2017, 12, 546-550.	15.6	1,364
4	Cross-sectional imaging of individual layers and buried interfaces of graphene-based heterostructures and superlattices. Nature Materials, 2012, 11, 764-767.	13.3	796
5	Production of few-layer phosphorene by liquid exfoliation of black phosphorus. Chemical Communications, 2014, 50, 13338-13341.	2.2	667
6	Molecular transport through capillaries made with atomic-scale precision. Nature, 2016, 538, 222-225.	13.7	483
7	Electronic Properties of Graphene Encapsulated with Different Two-Dimensional Atomic Crystals. Nano Letters, 2014, 14, 3270-3276.	4.5	433
8	Quality Heterostructures from Two-Dimensional Crystals Unstable in Air by Their Assembly in Inert Atmosphere. Nano Letters, 2015, 15, 4914-4921.	4.5	358
9	Desalination and Nanofiltration through Functionalized Laminar MoS <sub>2</sub> Membranes. ACS Nano, 2017, 11, 11082-11090.	7.3	275
10	Grain-Boundary-Enhanced Carrier Collection in CdTe Solar Cells. Physical Review Letters, 2014, 112, 156103.	2.9	258
11	Atomic reconstruction in twisted bilayers of transition metal dichalcogenides. Nature Nanotechnology, 2020, 15, 592-597.	15.6	245
12	WSe <sub>2</sub> Light-Emitting Tunneling Transistors with Enhanced Brightness at Room Temperature. Nano Letters, 2015, 15, 8223-8228.	4.5	231
13	Galvanic replacement reaction: recent developments for engineering metal nanostructures towards catalytic applications. Chemical Communications, 2017, 53, 7135-7148.	2.2	222
14	Tin(II) Sulfide (SnS) Nanosheets by Liquid-Phase Exfoliation of Herzenbergite: IV–VI Main Group Two-Dimensional Atomic Crystals. Journal of the American Chemical Society, 2015, 137, 12689-12696.	6.6	220
15	Nanostructured Aptamer-Functionalized Black Phosphorus Sensing Platform for Label-Free Detection of Myoglobin, a Cardiovascular Disease Biomarker. ACS Applied Materials & Interfaces, 2016, 8, 22860-22868.	4.0	208
16	Electrochemical properties of CVD grown pristine graphene: monolayer- vs. quasi-graphene. Nanoscale, 2014, 6, 1607-1621.	2.8	177
17	Capillary condensation under atomic-scale confinement. Nature, 2020, 588, 250-253.	13.7	168
18	Heterostructures Produced from Nanosheet-Based Inks. Nano Letters, 2014, 14, 3987-3992.	4.5	165

2

#	Article	IF	CITATIONS
19	Mechanisms of Liquid-Phase Exfoliation for the Production of Graphene. ACS Nano, 2020, 14, 10976-10985.	7.3	157
20	Caesium incorporation and retention in illite interlayers. Applied Clay Science, 2015, 108, 128-134.	2.6	155
21	Ballistic molecular transport through two-dimensional channels. Nature, 2018, 558, 420-424.	13.7	139
22	Van der Waals pressure and its effect on trapped interlayer molecules. Nature Communications, 2016, 7, 12168.	5.8	137
23	Synthesis of Lateral Size-Controlled Monolayer 1 <i>H-</i> MoS <sub>2</sub> @Oleylamine as Supercapacitor Electrodes Chemistry of Materials, 2016, 28, 657-664.	3.2	134
24	Synthesis and Structural Characterization of Branched Palladium Nanostructures. Advanced Materials, 2009, 21, 2288-2293.	11.1	124
25	Correlative Tomography. Scientific Reports, 2014, 4, 4711.	1.6	124
26	Correlating Catalytic Activity of Ag–Au Nanoparticles with 3D Compositional Variations. Nano Letters, 2014, 14, 1921-1926.	4.5	119
27	Investigation of dealloying of S phase (Al 2 CuMg) in AA 2024-T3 aluminium alloy using high resolution 2D and 3D electron imaging. Corrosion Science, 2016, 103, 157-164.	3.0	119
28	Interfacial ferroelectricity in marginally twisted 2D semiconductors. Nature Nanotechnology, 2022, 17, 390-395.	15.6	115
29	Biosynthesis and Characterization of Copper Nanoparticles Using <i>Shewanella oneidensis</i> : Application for Click Chemistry. Small, 2018, 14, 1703145.	5.2	112
30	Mechanistic study of non-thermal plasma assisted CO2 hydrogenation over Ru supported on MgAl layered double hydroxide. Applied Catalysis B: Environmental, 2020, 268, 118752.	10.8	101
31	Nanometer Resolution Elemental Mapping in Graphene-Based TEM Liquid Cells. Nano Letters, 2018, 18, 1168-1174.	4.5	99
32	Atomic-Scale Insights into the Oxidation of Aluminum. ACS Applied Materials & Interfaces, 2018, 10, 2230-2235.	4.0	95
33	The benefits of very low earth orbit for earth observation missions. Progress in Aerospace Sciences, 2020, 117, 100619.	6.3	95
34	Exfoliation of natural van der Waals heterostructures to a single unit cell thickness. Nature Communications, 2017, 8, 14410.	5.8	93
35	Micromagnetometry of two-dimensional ferromagnets. Nature Electronics, 2019, 2, 457-463.	13.1	93
36	Controlling Reaction Selectivity over Hybrid Plasmonic Nanocatalysts. Nano Letters, 2018, 18, 7289-7297.	4.5	92

#	Article	IF	CITATIONS
37	Nearâ€Unity Quantum Yields from Chloride Treated CdTe Colloidal Quantum Dots. Small, 2015, 11, 1548-1554.	5.2	86
38	In Situ Synthesis of PbS Nanocrystals in Polymer Thin Films from Lead(II) Xanthate and Dithiocarbamate Complexes: Evidence for Size and Morphology Control. Chemistry of Materials, 2015, 27, 2127-2136.	3.2	84
39	Compositional variations for small-scale gamma prime (γ′) precipitates formed at different cooling rates in an advanced Ni-based superalloy. Acta Materialia, 2015, 85, 199-206.	3.8	81
40	Thin Films of Molybdenum Disulfide Doped with Chromium by Aerosol-Assisted Chemical Vapor Deposition (AACVD). Chemistry of Materials, 2015, 27, 1367-1374.	3.2	78
41	Surface Properties of Nanocrystalline PbS Films Deposited at the Water–Oil Interface: A Study of Atmospheric Aging. Langmuir, 2015, 31, 1445-1453.	1.6	74
42	STEM-EDX tomography of bimetallic nanoparticles: A methodological investigation. Ultramicroscopy, 2016, 162, 61-73.	0.8	74
43	Self-assembly of a layered two-dimensional molecularly woven fabric. Nature, 2020, 588, 429-435.	13.7	74
44	Magnetoresistance of vertical Co-graphene-NiFe junctions controlled by charge transfer and proximity-induced spin splitting in graphene. 2D Materials, 2017, 4, 031004.	2.0	73
45	New routes to copper sulfide nanostructures and thin films. Journal of Materials Chemistry, 2011, 21, 17888.	6.7	70
46	The Effects of Extensive Glomerular Filtration of Thin Graphene Oxide Sheets on Kidney Physiology. ACS Nano, 2016, 10, 10753-10767.	7.3	70
47	An investigation of diffusion-mediated cyclic coarsening and reversal coarsening in an advanced Ni-based superalloy. Acta Materialia, 2016, 110, 295-305.	3.8	69
48	Reversible Loss of Bernal Stacking during the Deformation of Few-Layer Graphene in Nanocomposites. ACS Nano, 2013, 7, 7287-7294.	7.3	68
49	X-ray Energy-Dispersive Spectrometry During <i>In Situ</i> Liquid Cell Studies Using an Analytical Electron Microscope. Microscopy and Microanalysis, 2014, 20, 323-329.	0.2	66
50	Atomically Dispersed Copper Sites in a Metal–Organic Framework for Reduction of Nitrogen Dioxide. Journal of the American Chemical Society, 2021, 143, 10977-10985.	6.6	66
51	Real-time imaging and elemental mapping of AgAu nanoparticle transformations. Nanoscale, 2014, 6, 13598-13605.	2.8	64
52	Asymmetric MoS <sub>2</sub> /Graphene/Metal Sandwiches: Preparation, Characterization, and Application. Advanced Materials, 2016, 28, 8256-8264.	11.1	64
53	Atomic Defects and Doping of Monolayer NbSe <sub>2</sub> . ACS Nano, 2017, 11, 2894-2904.	7.3	63
54	Solution processing of two-dimensional black phosphorus. Chemical Communications, 2017, 53, 1445-1458.	2.2	63

#	Article	IF	CITATIONS
55	Indirect to Direct Gap Crossover in Two-Dimensional InSe Revealed by Angle-Resolved Photoemission Spectroscopy. ACS Nano, 2019, 13, 2136-2142.	7.3	63
56	In-situ observation and atomic resolution imaging of the ion irradiation induced amorphisation of graphene. Scientific Reports, 2014, 4, 6334.	1.6	62
57	Raman Fingerprints of Graphene Produced by Anodic Electrochemical Exfoliation. Nano Letters, 2020, 20, 3411-3419.	4.5	59
58	Enhanced organophilic separations with mixed matrix membranes of polymers of intrinsic microporosity and graphene-like fillers. Journal of Membrane Science, 2017, 526, 437-449.	4.1	57
59	Real-time imaging and local elemental analysis of nanostructures in liquids. Chemical Communications, 2014, 50, 10019-10022.	2.2	56
60	Comparison of solar cells sensitised by CdTe/CdSe and CdSe/CdTe core/shell colloidal quantum dots with and without a CdS outer layer. Thin Solid Films, 2014, 560, 65-70.	0.8	55
61	Segregation of In to Dislocations in InGaN. Nano Letters, 2015, 15, 923-930.	4.5	54
62	Stacking Order in Graphite Films Controlled by van der Waals Technology. Nano Letters, 2019, 19, 8526-8532.	4.5	54
63	Observing Imperfection in Atomic Interfaces for van der Waals Heterostructures. Nano Letters, 2017, 17, 5222-5228.	4.5	53
64	Infrared-to-violet tunable optical activity in atomic films of GaSe, InSe, and their heterostructures. 2D Materials, 2018, 5, 041009.	2.0	52
65	Laser-writable high-k dielectric for van der Waals nanoelectronics. Science Advances, 2019, 5, eaau0906.	4.7	51
66	Splenic Capture and <i>In Vivo</i> Intracellular Biodegradation of Biological-Grade Graphene Oxide Sheets. ACS Nano, 2020, 14, 10168-10186.	7.3	51
67	Purification of Propylene and Ethylene by a Robust Metal–Organic Framework Mediated by Host–Guest Interactions. Angewandte Chemie - International Edition, 2021, 60, 15541-15547.	7.2	51
68	Dielectric nanosheets made by liquid-phase exfoliation in water and their use in graphene-based electronics. 2D Materials, 2014, 1, 011012.	2.0	49
69	Iron redistribution in a zirconium alloy after neutron and proton irradiation studied by energy-dispersive X-ray spectroscopy (EDX) using an aberration-corrected (scanning) transmission electron microscope. Journal of Nuclear Materials, 2014, 454, 387-397.	1.3	49
70	Large magnetoelectric coupling in multiferroic oxide heterostructures assembled via epitaxial lift-off. Nature Communications, 2020, 11, 3190.	5.8	48
71	Self-catalytic membrane photo-reactor made of carbon nitride nanosheets. Journal of Materials Chemistry A, 2016, 4, 11666-11671.	5.2	47
72	Anomalous twin boundaries in two dimensional materials. Nature Communications, 2018, 9, 3597.	5.8	46

#	Article	IF	CITATIONS
73	MXene Tunable Lamellae Architectures for Supercapacitor Electrodes. ACS Applied Energy Materials, 2020, 3, 411-422.	2.5	46
74	Pillared Mo <sub>2</sub> TiC <sub>2</sub> MXene for high-power and long-life lithium and sodium-ion batteries. Nanoscale Advances, 2021, 3, 3145-3158.	2.2	46
75	The synthesis of metallic and semiconducting nanoparticles from reactive melts of precursors. Journal of Materials Chemistry A, 2014, 2, 570-580.	5.2	45
76	Measurement of size-dependent composition variations for gamma prime (γ′) precipitates in an advanced nickel-based superalloy. Ultramicroscopy, 2014, 144, 1-8.	0.8	45
77	Transport of hydrogen isotopes through interlayer spacing in van der Waals crystals. Nature Nanotechnology, 2018, 13, 468-472.	15.6	45
78	Atomically thin micas as proton-conducting membranes. Nature Nanotechnology, 2019, 14, 962-966.	15.6	45
79	RF Helicon-based Inductive Plasma Thruster (IPT) Design for an Atmosphere-Breathing Electric Propulsion system (ABEP). Acta Astronautica, 2020, 176, 476-483.	1.7	45
80	Scalable Patterning of Encapsulated Black Phosphorus. Nano Letters, 2018, 18, 5373-5381.	4.5	43
81	Nonreciprocal superconducting NbSe2 antenna. Nature Communications, 2020, 11, 5634.	5.8	43
82	Controlling Size, Morphology, and Surface Composition of AgAu Nanodendrites in 15 s for Improved Environmental Catalysis under Low Metal Loadings. ACS Applied Materials & Interfaces, 2015, 7, 25624-25632.	4.0	42
83	Sequential bottom-up and top-down processing for the synthesis of transition metal dichalcogenide nanosheets: the case of rhenium disulfide (ReS <sub>2</sub> ). Chemical Communications, 2016, 52, 7878-7881.	2.2	42
84	A review of gas-surface interaction models for orbital aerodynamics applications. Progress in Aerospace Sciences, 2020, 119, 100675.	6.3	41
85	MoS <sub>2</sub> nanosheet production by the direct exfoliation of molybdenite minerals from several type-localities. RSC Advances, 2014, 4, 35609-35613.	1.7	40
86	Metal-organic framework templated electrodeposition of functional gold nanostructures. Electrochimica Acta, 2016, 222, 361-369.	2.6	40
87	Ion exchange in atomically thin clays and micas. Nature Materials, 2021, 20, 1677-1682.	13.3	40
88	Au@HgxCd1-xTe core@shell nanorods by sequential aqueous cation exchange for near-infrared photodetectors. Nano Energy, 2019, 57, 57-65.	8.2	38
89	Direct synthesis of MoS <sub>2</sub> or MoO <sub>3</sub> <i>via</i> thermolysis of a dialkyl dithiocarbamato molybdenum( <scp>iv</scp> ) complex. Chemical Communications, 2019, 55, 99-102.	2.2	38
90	The application of in situ analytical transmission electron microscopy to the study of preferential intergranular oxidation in Alloy 600. Ultramicroscopy, 2017, 176, 46-51.	0.8	37

#	Article	IF	CITATIONS
91	Oleylamine Aging of PtNi Nanoparticles Giving Enhanced Functionality for the Oxygen Reduction Reaction. Nano Letters, 2021, 21, 3989-3996.	4.5	37
92	Quantitative Energy-Dispersive X-Ray Analysis of Catalyst Nanoparticles Using a Partial Cross Section Approach. Microscopy and Microanalysis, 2016, 22, 71-81.	0.2	36
93	Heterostructures formed through abraded van der Waals materials. Nature Communications, 2020, 11, 3047.	5.8	36
94	High-performance polymer electrolyte membranes incorporated with 2D silica nanosheets in high-temperature proton exchange membrane fuel cells. Journal of Energy Chemistry, 2022, 64, 323-334.	7.1	36
95	Gold–Rhodium Nanoflowers for the Plasmon-Enhanced Hydrogen Evolution Reaction under Visible Light. ACS Catalysis, 2021, 11, 13543-13555.	5.5	36
96	Formation and Healing of Defects in Atomically Thin GaSe and InSe. ACS Nano, 2019, 13, 5112-5123.	7.3	35
97	Iron, Nitrogen Coâ€Doped Carbon Spheres as Low Cost, Scalable Electrocatalysts for the Oxygen Reduction Reaction. Advanced Functional Materials, 2021, 31, 2102974.	7.8	35
98	Synthesis and characterization of composite membranes made of graphene and polymers of intrinsic microporosity. Carbon, 2016, 102, 357-366.	5.4	34
99	CVDgraphenevs. highly ordered pyrolytic graphite for use in electroanalytical sensing. Analyst, The, 2012, 137, 833-839.	1.7	33
100	Dynamic microstructural evolution of graphite under displacing irradiation. Carbon, 2014, 68, 273-284.	5.4	33
101	Multiscale correlative tomography: an investigation of creep cavitation in 316 stainless steel. Scientific Reports, 2017, 7, 7332.	1.6	33
102	Ultra-thin van der Waals crystals as semiconductor quantum wells. Nature Communications, 2020, 11, 125.	5.8	33
103	Intake design for an Atmosphere-Breathing Electric Propulsion System (ABEP). Acta Astronautica, 2021, 187, 225-235.	1.7	33
104	A Conspicuous Clay Ovoid in Nakhla: Evidence for Subsurface Hydrothermal Alteration on Mars with Implications for Astrobiology. Astrobiology, 2014, 14, 651-693.	1.5	32
105	Two-Dimensional Covalent Crystals by Chemical Conversion of Thin van der Waals Materials. Nano Letters, 2019, 19, 6475-6481.	4.5	32
106	Non-rigid registration and non-local principle component analysis to improve electron microscopy spectrum images. Nanotechnology, 2016, 27, 364001.	1.3	30
107	Porous Silica-Pillared MXenes with Controllable Interlayer Distances for Long-Life Na-Ion Batteries. Langmuir, 2020, 36, 4370-4382.	1.6	30
108	Comparing Xe <sup>+</sup> pFIB and Ga <sup>+</sup> FIB for TEM sample preparation of Al alloys: Minimising FIBâ€induced artefacts. Journal of Microscopy, 2021, 282, 101-112.	0.8	29

#	Article	IF	CITATIONS
109	S–Te Interdiffusion within Grains and Grain Boundaries in CdTe Solar Cells. IEEE Journal of Photovoltaics, 2014, 4, 1636-1643.	1.5	28
110	Single-Source Precursor for Tungsten Dichalcogenide Thin Films: Mo <sub>1–<i>x</i></sub> W <sub><i>x</i></sub> S <sub>2</sub> (0 ≤i>x ≤) Alloys by Aerosol-Assisted Chemical Vapor Deposition. Chemistry of Materials, 2017, 29, 3858-3862.	3.2	28
111	Black phosphorus with near-superhydrophobic properties and long-term stability in aqueous media. Chemical Communications, 2018, 54, 3831-3834.	2.2	28
112	Surfactant-free Synthesis of Spiky Hollow Ag–Au Nanostars with Chemically Exposed Surfaces for Enhanced Catalysis and Single-Particle SERS. Jacs Au, 2022, 2, 178-187.	3.6	28
113	Chemical interactions in Ti doped MgB2superconducting bulk samples and wires. Superconductor Science and Technology, 2005, 18, 1190-1196.	1.8	27
114	Total Ionizing Dose Effects on hBN Encapsulated Graphene Devices. IEEE Transactions on Nuclear Science, 2014, 61, 2868-2873.	1.2	27
115	Controlled Folding of Graphene: GraFold Printing. Nano Letters, 2015, 15, 857-863.	4.5	27
116	Role of 2D and 3D defects on the reduction of LaNiO3 nanoparticles for catalysis. Scientific Reports, 2017, 7, 10080.	1.6	27
117	In-orbit aerodynamic coefficient measurements using SOAR (Satellite for Orbital Aerodynamics) Tj ETQq1 1 0.78	4314 rgB <sup>-</sup> 1.7	[ /Qyerlock 10
118	Atomic Structure Imaging Beyond Conventional Resolution Limits in the Transmission Electron Microscope. Physical Review Letters, 2009, 103, 126101.	2.9	26
119	Formation of barrier-type anodic films on ZE41 magnesium alloy in a fluoride/glycerol electrolyte. Electrochimica Acta, 2014, 138, 124-131.	2.6	26
120	Nano-particle precipitation in mechanically alloyed and annealed precursor powders of legacy PM2000 ODS alloy. Journal of Nuclear Materials, 2015, 464, 200-209.	1.3	24
121	Multiscale 3D analysis of creep cavities in AISI type 316 stainless steel. Materials Science and Technology, 2015, 31, 522-534.	0.8	24
122	Chemical vapor deposition of tin sulfide from diorganotin(IV) dixanthates. Journal of Materials Science, 2019, 54, 2315-2323.	1.7	24
123	Stability and stoichiometry of L12 Al3(Sc,Zr) dispersoids in Al-(Si)-Sc-Zr alloys. Acta Materialia, 2021, 216, 117117.	3.8	24
124	Dual Functionalization of Liquidâ€Exfoliated Semiconducting 2 <i>Hâ€</i> MoS <sub>2</sub> with Lanthanide Complexes Bearing Magnetic and Luminescence Properties. Advanced Functional Materials, 2017, 27, 1703646.	7.8	23
125	Synthesis of Bi <sub>2â~'2x</sub> Sb <sub>2x</sub> S <sub>3</sub> (0 ≤i>x ≤) solid solutions from solventless thermolysis of metal xanthate precursors. Journal of Materials Chemistry C, 2018, 6, 12652-12659.	2.7	23
126	Enhanced Superconductivity in Few-Layer TaS <sub>2</sub> due to Healing by Oxygenation. Nano Letters, 2020, 20, 3808-3818.	4.5	23

SARAH HAIGH

#	Article	IF	CITATIONS
127	Solution-Processed HfO <sub><i>x</i></sub> for Half-Volt Operation of InGaZnO Thin-Film Transistors. ACS Applied Electronic Materials, 2019, 1, 1581-1589.	2.0	22

Synthesis of new M-layer solid-solution 312 MAX phases (Ta<sub>1â<sup>^</sup><i>x</i>/sub>Ti<sub><i>x</i>/sub>Sib>3</sub>AlC<sub>2</sub> (<i>x</i> = 0.4, 0.62,) Tj ETQqΩΩ 0 rgBTzbQverlock 128

129	An in situ and ex situ TEM study into the oxidation of titanium (IV) sulphide. Npj 2D Materials and Applications, 2017, 1, .	3.9	21
130	Imaging the Active Surfaces of Cerium Dioxide Nanoparticles. ChemPhysChem, 2011, 12, 2397-2399.	1.0	20
131	Hydrogen evolution and capacitance behavior of Au/Pd nanoparticle-decorated graphene heterostructures. Applied Materials Today, 2017, 8, 125-131.	2.3	20
132	Confinement Effects and Charge Dynamics in Zn <sub>3</sub> N <sub>2</sub> Colloidal Quantum Dots: Implications for QD-LED Displays. ACS Applied Nano Materials, 2019, 2, 7214-7219.	2.4	20
133	Design-controlled synthesis of IrO <sub>2</sub> sub-monolayers on Au nanoflowers: marrying plasmonic and electrocatalytic properties. Nanoscale, 2020, 12, 12281-12291.	2.8	20
134	A structured catalyst support combining electrochemically exfoliated graphene oxide and carbon black for enhanced performance and durability in low-temperature hydrogen fuel cells. Energy, 2021, 226, 120318.	4.5	20
135	Unraveling the H <sub>2</sub> Promotional Effect on Palladium-Catalyzed CO Oxidation Using a Combination of Temporally and Spatially Resolved Investigations. ACS Catalysis, 2018, 8, 8255-8262.	5.5	19
136	The influence of precursor on rhenium incorporation into Re-doped MoS <sub>2</sub> (Mo <sub>1â^'x</sub> Re <sub>x</sub> S <sub>2</sub> ) thin films by aerosol-assisted chemical vapour deposition (AACVD). Journal of Materials Chemistry C, 2017, 5, 9044-9052.	2.7	18
137	Imaging Three-Dimensional Elemental Inhomogeneity in Pt–Ni Nanoparticles Using Spectroscopic Single Particle Reconstruction. Nano Letters, 2019, 19, 732-738.	4.5	18
138	Self-Limiting Growth of Two-Dimensional Palladium between Graphene Oxide Layers. Nano Letters, 2019, 19, 4678-4683.	4.5	18
139	In Situ TEM Imaging of Solutionâ€Phase Chemical Reactions Using 2Dâ€Heterostructure Mixing Cells. Advanced Materials, 2021, 33, e2100668.	11.1	18
140	Optimal tilt magnitude determination for aberration-corrected super resolution exit wave function reconstruction. Philosophical Transactions Series A, Mathematical, Physical, and Engineering Sciences, 2009, 367, 3755-3771.	1.6	17
141	Atomic resolution electrostatic potential mapping of graphene sheets by off-axis electron holography. Journal of Applied Physics, 2014, 115, .	1.1	17
142	Ultrastructure and Crystallography of Nanoscale Calcite Building Blocks in <i>Rhabdosphaera clavigera</i> Coccolith Spines. Crystal Growth and Design, 2014, 14, 1710-1718.	1.4	17
143	Surface Segregated AgAu Tadpoleâ€5haped Nanoparticles Synthesized Via a Single Step Combined Galvanic and Citrate Reduction Reaction. Chemistry - A European Journal, 2015, 21, 12314-12320.	1.7	17
144	Convergent beam electron holography for analysis of van der Waals heterostructures. Proceedings of the National Academy of Sciences of the United States of America, 2018, 115, 7473-7478.	3.3	17

#	Article	IF	CITATIONS
145	Synthesis of copper catalysts for click chemistry from distillery wastewater using magnetically recoverable bionanoparticles. Green Chemistry, 2019, 21, 4020-4024.	4.6	17
146	Characterising porosity in platinum nanoparticles. Nanoscale, 2019, 11, 17791-17799.	2.8	17
147	Photocatalytic hydrogen production by biomimetic indium sulfide using Mimosa pudica leaves as template. International Journal of Hydrogen Energy, 2019, 44, 2770-2783.	3.8	17
148	Dislocation core structures in (0001) InGaN. Journal of Applied Physics, 2016, 119, .	1.1	16
149	Synthetic 2-D lead tin sulfide nanosheets with tuneable optoelectronic properties from a potentially scalable reaction pathway. Chemical Science, 2019, 10, 1035-1045.	3.7	16
150	Electrically pumped WSe2-based light-emitting van der Waals heterostructures embedded in monolithic dielectric microcavities. 2D Materials, 2020, 7, 031006.	2.0	16
151	High-Resolution TEM and the Application of Direct and Indirect Aberration Correction. Microscopy and Microanalysis, 2008, 14, 60-67.	0.2	15
152	In Situ Industrial Bimetallic Catalyst Characterization using Scanning Transmission Electron Microscopy and Xâ€ray Absorption Spectroscopy at One Atmosphere and Elevated Temperature. ChemPhysChem, 2017, 18, 2151-2156.	1.0	15
153	Magnetoresistance in Co-hBN-NiFe Tunnel Junctions Enhanced by Resonant Tunneling through Single Defects in Ultrathin hBN Barriers. Nano Letters, 2018, 18, 6954-6960.	4.5	15
154	Beyond surface redox and oxygen mobility at pd-polar ceria (100) interface: Underlying principle for strong metal-support interactions in green catalysis. Applied Catalysis B: Environmental, 2020, 270, 118843.	10.8	15
155	Correlation of the ratio of metallic to oxide species with activity of PdPt catalysts for methane oxidation. Catalysis Science and Technology, 2020, 10, 1408-1421.	2.1	15
156	Gas permeation through graphdiyne-based nanoporous membranes. Nature Communications, 2022, 13, .	5.8	15
157	Recording low and high spatial frequencies in exit wave reconstructions. Ultramicroscopy, 2013, 133, 26-34.	0.8	14
158	High magnetic relaxivity in a fluorescent CdSe/CdS/ZnS quantum dot functionalized with MRI contrast molecules. Chemical Communications, 2017, 53, 10500-10503.	2.2	14
159	Diatom Frustules as a Biomineralized Scaffold for the Growth of Molybdenum Disulfide Nanosheets. Chemistry of Materials, 2016, 28, 5582-5586.	3.2	13
160	Liquid Exfoliation of Ni <sub>2</sub> P <sub>2</sub> S <sub>6</sub> : Structural Characterization, Size-Dependent Properties, and Degradation. Chemistry of Materials, 2019, 31, 9127-9139.	3.2	13
161	Rapid and Low-Temperature Molecular Precursor Approach toward Ternary Layered Metal Chalcogenides and Oxides: Mo <sub>1–<i>x</i></sub> W <sub><i>x</i></sub> S <sub>2</sub> and Mo <sub>1–<i>x</i></sub> W <sub><i>x</i></sub> O <sub>3</sub> Alloys (0 ≤i>x ≤). Chemistry of Materials. 2020. 32. 7895-7907.	3.2	13
162	Atomic Resolution Imaging of CrBr3 Using Adhesion-Enhanced Grids. Nano Letters, 2020, 20, 6582-6589.	4.5	13

#	Article	IF	CITATIONS
163	An in-situ method for protecting internal cracks/pores from ion beam damage and reducing curtaining for TEM sample preparation using FIB. Ultramicroscopy, 2020, 219, 113135.	0.8	13
164	Automated Single-Particle Reconstruction of Heterogeneous Inorganic Nanoparticles. Microscopy and Microanalysis, 2020, 26, 1168-1175.	0.2	13
165	Understanding the limitations of the Super-X energy dispersive x-ray spectrometer as a function of specimen tilt angle for tomographic data acquisition in the S/TEM. Journal of Physics: Conference Series, 2014, 522, 012025.	0.3	12
166	Transmission electron microscopy without aberrations: Applications to materials science. Current Applied Physics, 2008, 8, 425-428.	1.1	11
167	Bilayer graphene formed by passage of current through graphite: evidence for a three-dimensional structure. Nanotechnology, 2014, 25, 465601.	1.3	11
168	Preparation of low-dimensional carbon material-based metal nanocomposites using a polarizable organic/water interface. Journal of Materials Research, 2015, 30, 2679-2687.	1.2	11
169	Compositional quantification of PtCo acid-leached fuel cell catalysts using EDX partial cross sections. Materials Science and Technology, 2016, 32, 248-253.	0.8	11
170	Development and analysis of novel mission scenarios based on Atmosphere-Breathing Electric Propulsion (ABEP). CEAS Space Journal, 2022, 14, 689-706.	1.1	11
171	Precise control of interface anisotropy during deposition of Co/Pd multilayers. Journal of Applied Physics, 2014, 116, .	1.1	10
172	Nanometre electron beam sculpting of suspended graphene and hexagonal boron nitride heterostructures. 2D Materials, 2019, 6, 025032.	2.0	10
173	Controlling Interfacial Reduction Kinetics and Suppressing Electrochemical Oscillations in Li <sub>4</sub> Ti <sub>5</sub> O <sub>12</sub> Thinâ€Film Anodes. Advanced Functional Materials, 2021, 31, 2105354.	7.8	10
174	Compositional variations in In <sub>0.5</sub> Ga <sub>0.5</sub> N nanorods grown by molecular beam epitaxy. Nanotechnology, 2014, 25, 215705.	1.3	9
175	Magnetic spectroscopy of nanoparticulate greigite, Fe <sub>3</sub> S <sub>4</sub> . Mineralogical Magazine, 2017, 81, 857-872.	0.6	9
176	Electrocatalytic Behavior of PtCu Clusters Produced by Nanoparticle Beam Deposition. Journal of Physical Chemistry C, 2020, 124, 23683-23689.	1.5	9
177	High-Performance Nanostructured MoS <sub>2</sub> Electrodes with Spontaneous Ultralow Gold Loading for Hydrogen Evolution. Journal of Physical Chemistry C, 2021, 125, 20940-20951.	1.5	9
178	Nanocubes of Mo <sub>6</sub> S <sub>8</sub> Chevrel phase as active electrode material for aqueous lithium-ion batteries. Nanoscale, 2022, 14, 10125-10135.	2.8	9
179	Ultrahigh resolution imaging of local structural distortions in intergrowth tungsten bronzes. Ultramicroscopy, 2007, 107, 501-506.	0.8	8
180	Exit wave reconstruction from focal series of HRTEM images, single crystal XRD and total energy studies on Sb <sub><i>x</i></sub> WO <sub>3+<i>y</i></sub> ( <i>x</i> â^1⁄4 0.11). Zeitschrift Fur Kristallographie - Crystalline Materials, 2012, 227, 341-349.	0.4	8

#	Article	IF	CITATIONS
181	Kink Band Formation in Graphite under Ion Irradiation at 100 and 298 K. Materials Transactions, 2014, 55, 447-450.	0.4	8
182	XEDS and EELS in the TEM at Atmospheric Pressure and High Temperature. Microscopy and Microanalysis, 2015, 21, 247-248.	0.2	8
183	Direct measurement of TEM lamella thickness in FIB EM. Journal of Microscopy, 2020, 279, 168-176.	0.8	8
184	Hydrotalcite Colloidal Stability and Interactions with Uranium(VI) at Neutral to Alkaline pH. Langmuir, 2022, 38, 2576-2589.	1.6	8
185	Exceeding Conventional Resolution Limits in High-Resolution Transmission Electron Microscopy Using Tilted Illumination and Exit-Wave Restoration. Microscopy and Microanalysis, 2010, 16, 409-415.	0.2	7
186	Optimized conditions for imaging the effects of bonding charge density in electron microscopy. Ultramicroscopy, 2011, 111, 901-911.	0.8	7
187	Investigation of the GaN-on-GaAs interface for vertical power device applications. Journal of Applied Physics, 2014, 116, .	1.1	7
188	A Facile Strategy to Support Palladium Nanoparticles on Carbon Nanotubes, Employing Polyvinylpyrrolidone as a Surface Modifier. European Journal of Inorganic Chemistry, 2014, 2014, 1439-1445.	1.0	7
189	Radiation damage in biotite mica by accelerated α-particles: A synchrotron microfocus X-ray diffraction and X-ray absorption spectroscopy studyk. American Mineralogist, 2016, 101, 928-942.	0.9	7
190	X-Ray Absorption Correction for Quantitative Scanning Transmission Electron Microscopic Energy-Dispersive X-Ray Spectroscopy of Spherical Nanoparticles. Microscopy and Microanalysis, 2016, 22, 440-447.	0.2	7
191	Cu segregation on the interface between Al 2 O 3 substrate and Al-1.4Cu alloy. Materials Characterization, 2017, 129, 300-304.	1.9	7
192	Convergent and divergent beam electron holography and reconstruction of adsorbates on free-standing two-dimensional crystals. Frontiers of Physics, 2019, 14, 1.	2.4	7
193	Hydrocarbon contamination in angström-scale channels. Nanoscale, 2021, 13, 9553-9560.	2.8	7
194	Telluride Nanocrystals with Adjustable Amorphous Shell Thickness and Core–Shell Structure Modulation by Aqueous Cation Exchange. Inorganic Chemistry, 2022, 61, 3989-3996.	1.9	7
195	Lowâ€Temperature Exsolution of Ni–Ru Bimetallic Nanoparticles from A‣ite Deficient Double Perovskites. Small, 2022, 18, e2107020.	5.2	7
196	High-Pressure High-Temperature Synthesis of Nanostructural Magnesium Diboride for Electromotors and Devices Working at Liquid Hydrogen Temperatures. Advances in Science and Technology, 2006, 47, 25.	0.2	6
197	Chapter 8 Aberration-Corrected Imaging in Conventional Transmission Electron Microscopy and Scanning Transmission Electron Microscopy. Advances in Imaging and Electron Physics, 2008, , 283-325.	0.1	6
198	Synthesis of biocompatible Au–ZnTe core–shell nanoparticles. Journal of Materials Chemistry B, 2015, 3, 2826-2833.	2.9	6

#	Article	IF	CITATIONS
199	The Biosynthesis of Infrared-Emitting Quantum Dots in Allium Fistulosum. Scientific Reports, 2016, 6, 20480.	1.6	6
200	Gas-Phase Deposition of Gold Nanoclusters to Produce Heterogeneous Glycerol Oxidation Catalysts. ACS Applied Nano Materials, 2020, 3, 4997-5001.	2.4	6
201	Convergent beam electron diffraction of multilayer Van der Waals structures. Ultramicroscopy, 2020, 212, 112976.	0.8	6
202	Nanometre imaging of Fe <sub>3</sub> GeTe <sub>2</sub> ferromagnetic domain walls. Nanotechnology, 2021, 32, 205703.	1.3	6
203	Iron-silica interaction during reduction of precipitated silica-promoted iron oxides using in situ XRD and TEM. Applied Catalysis A: General, 2021, 613, 118031.	2.2	6
204	Behavior of Alloying Elements during Anodizing of Mg-Cu and Mg-W Alloys in a Fluoride/Glycerol Electrolyte. Journal of the Electrochemical Society, 2015, 162, C487-C494.	1.3	5
205	Radiation damage haloes in biotite investigated using high-resolution transmission electron microscopy. American Mineralogist, 2016, 101, 105-110.	0.9	5
206	Morphological and compositional changes of MFe2O4@Co3O4 (M = Ni, Zn) core-shell nanoparticles after mild reduction. Materials Characterization, 2019, 155, 109806.	1.9	5
207	Reply to: Random interstratification in hydrated graphene oxide membranes and implications for seawater desalination. Nature Nanotechnology, 2022, 17, 134-135.	15.6	5
208	Elucidating heterogeneous iron biomineralization patterns in a denitrifying As( <scp>iii</scp> )-oxidizing bacterium: implications for arsenic immobilization. Environmental Science: Nano, 2022, 9, 1076-1090.	2.2	5
209	High-resolution imaging of biotite using focal series exit wavefunction restoration and the graphene mechanical exfoliation method. Mineralogical Magazine, 2015, 79, 337-344.	0.6	4
210	Energy Dispersive X-ray Tomography for 3D Elemental Mapping of Individual Nanoparticles. Journal of Visualized Experiments, 2016, , .	0.2	4
211	Elemental distribution within the long-period stacking ordered structure in a Mg-Gd-Zn-Mn alloy. Materials Characterization, 2017, 129, 247-251.	1.9	4
212	Fate of Lu(III) sorbed on 2-line ferrihydrite at pHÂ5.7 and aged for 12Âyears at room temperature. II: insights from STEM-EDXS and DFT calculations. Environmental Science and Pollution Research, 2019, 26, 5282-5293.	2.7	4
213	Performance of a NiFe <sub>2</sub> O <sub>4</sub> @Co Core–Shell Fischer–Tropsch Catalyst: Effect of Low Temperature Reduction. ACS Omega, 2020, 5, 32975-32983.	1.6	4
214	Photo―and Electroluminescence from Znâ€Doped InN Semiconductor Nanocrystals. Advanced Optical Materials, 2020, 8, 2000604.	3.6	4
215	Synthesis of molybdenum-doped rhenium disulfide alloy using aerosol-assisted chemical vapour deposition. Materials Science in Semiconductor Processing, 2021, 127, 105718.	1.9	4
216	Controlling and Monitoring Crack Propagation in Monolayer Graphene Single Crystals. Advanced Functional Materials, 2022, 32, .	7.8	4

#	Article	IF	CITATIONS
217	High Resolution ExitWave Restoration. Nanostructure Science and Technology, 2012, , 41-72.	0.1	3
218	Probing the core-shell-shell structure of CdSe/CdTe/CdS type II quantum dots for solar cell applications. Journal of Physics: Conference Series, 2014, 522, 012069.	0.3	3
219	Bimetallic Au@Pdâ€Au Tadpoleâ€Shaped Asymmetric Nanostructures by a Combination of Precursor Reduction and Ostwald Ripening. ChemNanoMat, 2016, 2, 509-514.	1.5	3
220	Plasmon-induced nanoscale quantised conductance filaments. Scientific Reports, 2017, 7, 2878.	1.6	3
221	Automated quantification of morphology and chemistry from STEM data of individual nanoparticles. Journal of Physics: Conference Series, 2017, 902, 012018.	0.3	3
222	Core–shell–shell cytocompatible polymer dot-based particles with near-infrared emission and enhanced dispersion stability. Chemical Communications, 2018, 54, 9364-9367.	2.2	3
223	Magnetic-Field-Induced Re-entrance of Superconductivity in Ta2PdS5 Nanostrips. Nano Letters, 2021, 21, 288-297.	4.5	3
224	Chlorosulfuric acid-assisted production of functional 2D materials. Npj 2D Materials and Applications, 2021, 5, .	3.9	3
225	The modified liquid   liquid interface: An electrochemical route for the electrode-less synthesis of MoS2 metal composite thin films. Electrochimica Acta, 2022, 424, 140609.	2.6	3
226	Atom-by-Atom STEM Investigation of Defect Engineering in Graphene. Microscopy and Microanalysis, 2014, 20, 1736-1737.	0.2	2
227	In situ Analytical TEM of Ilmenite Reduction in Hydrogen. Microscopy and Microanalysis, 2015, 21, 565-566.	0.2	2
228	Imaging the Hydrated Microbe-Metal Interface Using Nanoscale Spectrum Imaging. Particle and Particle Systems Characterization, 2016, 33, 833-841.	1.2	2
229	Liquid-Phase STEM-EDS in Graphene and Silicon Nitride Cells. Microscopy and Microanalysis, 2019, 25, 1500-1501.	0.2	2
230	Holographic reconstruction of the interlayer distance of bilayer two-dimensional crystal samples from their convergent beam electron diffraction patterns. Ultramicroscopy, 2020, 219, 113020.	0.8	2
231	Finding phase information in the darkness. Journal of Physics: Conference Series, 2010, 241, 012013.	0.3	1
232	Recent developments in transmission electron microscopy and their application for nanoparticle characterisation. SPR Nanoscience, 2012, , 89-101.	0.3	1
233	Understanding Individual Defects in CdTe Solar Cells: From Atomic Structure to Electrical Activity. Microscopy and Microanalysis, 2014, 20, 518-519.	0.2	1
234	On the diffusion mechanisms of fine-scaleγ′ in an advanced Ni-based superalloy. MATEC Web of Conferences, 2014, 14, 09002.	0.1	1

#	Article	IF	CITATIONS
235	Cross sectional STEM imaging and analysis of multilayered two dimensional crystal heterostructure devices. Microscopy and Microanalysis, 2015, 21, 107-108.	0.2	1
236	Advanced Analytical Electron Microscopy: New Perspectives on Real Materials. Microscopy and Microanalysis, 2015, 21, 489-490.	0.2	1
237	Temperature Programmed Reduction of a PdCu Bimetallic Catalyst via Atmospheric Pressure in situ STEM-EDS and in situ X-Ray Adsorption Analysis. Microscopy and Microanalysis, 2016, 22, 214-215.	0.2	1
238	Energy Dispersive X-Ray Spectroscopy in Liquids: Inorganic and Biological Applications. Microscopy and Microanalysis, 2016, 22, 72-73.	0.2	1
239	Magic under the microscope. Nature Materials, 2021, 20, 908-909.	13.3	1
240	Automating 3D Imaging of Inorganic Nanoparticles. Microscopy and Microanalysis, 2021, 27, 2864-2866.	0.2	1
241	Aberration Correction and Exit Wave Reconstruction Using Tilt Azimuth Data. Microscopy and Microanalysis, 2009, 15, 1472-1473.	0.2	0
242	Real-space Measurements of Bonding Charge Density in Aberration-corrected High Resolution Electron Microscopy. Microscopy and Microanalysis, 2009, 15, 1478-1479.	0.2	0
243	Inside Cover: Imaging the Active Surfaces of Cerium Dioxide Nanoparticles (ChemPhysChem 13/2011). ChemPhysChem, 2011, 12, 2358-2358.	1.0	0
244	Direct Measurement of the Crystallographically Sensitive Atomic Termination of Nanophase Cerium Dioxide. Journal of Physics: Conference Series, 2012, 371, 012072.	0.3	0
245	A Facile Strategy to Support Palladium Nanoparticles on Carbon Nanotubes, Employing Polyvinylpyrrolidone as a Surface Modifier. European Journal of Inorganic Chemistry, 2014, 2014, 1422-1422.	1.0	0
246	New capabilities for `colouring in' the chemistry of crystal defects atom-by-atom. Acta Crystallographica Section A: Foundations and Advances, 2014, 70, 521-523.	0.0	0
247	Applications of Aberration Corrected TEM and Exit Wavefunction Reconstruction to Materials Science. Microscopy and Microanalysis, 2014, 20, 930-931.	0.2	0
248	Revealing New Atomic-scale Information about Materials by Improving the Quality and Quantifiability of Aberration-corrected STEM Data. Microscopy and Microanalysis, 2015, 21, 2409-2410.	0.2	0
249	Photoluminescence: Nearâ€Unity Quantum Yields from Chloride Treated CdTe Colloidal Quantum Dots (Small 13/2015). Small, 2015, 11, 1482-1482.	5.2	0
250	Frontispiece: Surface Segregated AgAu Tadpole-Shaped Nanoparticles Synthesized Via a Single Step Combined Galvanic and Citrate Reduction Reaction. Chemistry - A European Journal, 2015, 21, n/a-n/a.	1.7	0
251	Combining Non-Rigid Registration with Non-Local Principle Component Analysis for Atomic Resolution EDS Mapping. Microscopy and Microanalysis, 2016, 22, 1406-1407.	0.2	0
252	Understanding 2D Crystal Vertical Heterostructures at the Atomic Scale Using Advanced Scanning Transmission Electron Microscopy. Microscopy and Microanalysis, 2017, 23, 1714-1715.	0.2	0

#	Article	IF	CITATIONS
253	Analysis of grain size in FePt films fabricated using remote plasma deposition. Journal of Magnetism and Magnetic Materials, 2017, 443, 67-72.	1.0	0
254	Photo-oxidized HfS2 - An embeddable and writable high-k dielectric for flexible Van der Waals nano-electronics. , 2018, , .		0
255	Two Methods for Measuring Lamellae Thicknesses In situ for Improved FIB Specimen Preparation. Microscopy and Microanalysis, 2019, 25, 858-859.	0.2	0
256	Three-Dimensional Imaging of Nanoparticle Chemistry Using Spectroscopic Single Particle Reconstruction. Microscopy and Microanalysis, 2019, 25, 400-401.	0.2	0
257	Twist and Bend in Van Der Waals Materials and 2D Stacked Heterostructures. Microscopy and Microanalysis, 2020, 26, 856-858.	0.2	0
258	Guest Editor's Foreword, Special Issue Introduction and Scientific Highlights. Journal of Microscopy, 2020, 279, 141-142.	0.8	0
259	Harnessing the Electron Beam to Study Reactions in Graphene Liquid Cells and Degradation in Sensitive 2D Materials. Microscopy and Microanalysis, 2020, 26, 538-541.	0.2	0
260	Synthesis of IR-emitting HgTe quantum dots using an ionic liquid-based tellurium precursor. Nanoscale Advances, 2021, 3, 4062-4064.	2.2	0
261	HOLOGRAPHIC CONVERGENT ELECTRON BEAM DIFFRACTION (CBED) IMAGING OF TWO-DIMENSIONAL CRYSTALS. Surface Review and Letters, 2021, 28, 2140001.	0.5	0
262	Co-precipitation on the Basal and Prismatic Planes in Mg–Gd–Ag–Zr Alloy Subjected to Over-Ageing. Minerals, Metals and Materials Series, 2018, , 379-383.	0.3	0
263	Exploring Nanoscale Precursor Reactions in Alloy 600 in H2/N2–H2O Vapor Using In Situ Analytical Transmission Electron Microscopy, Minerals, Metals and Materials Series, 2018, , 399-407.	0.3	0